09

Fabrication of a blazed diffraction grating with variable line space

© D.V. Mokhov,[1,2] T.N. Berezovskaya,[1] K.Yu. Shubina,[1] E.V. Pirogov,[1] N.D. Prasolov,[3] L.I. Goray,[1,2,4,5] A.D. Bouravleuv[2,3,4]

[1] Alferov University, RAS,
194021 St. Petersburg, Russia
[2] St. Petersburg State Electrotechnical University „LETI" named after V.I.Ulyanov (Lenin),
197022 St. Petersburg, Russia
[3] Ioffe Institute,
194021 St. Petersburg, Russia
[4] Institute of Analytical Instrument Making, Russian Academy of Sciences,
198095 St. Petersburg, Russia
[5] Institute of Space Research, Russian Academy of Sciences,
117997 Moscow, Russia
e-mail: dm_mokhov@rambler.ru

Received April 29, 2025
Revised April 29, 2025
Accepted April 29, 2025

Variable line spacing (VLS) blazed gratings were fabricated on silicon substrates using direct laser lithography and anisotropic wet etching. The grating parameters were monitored during fabrication using scanning electron microscopy and atomic force microscopy. The paper reports on the fabrication details and characteristics of VLS-grating prototypes with different blaze angles for a solar-blind UV polychromator.

Keywords: Si diffraction grating, variable line spacing grating, blaze angle, triangle line profile, atomic force microscopy, scanning electron microscopy, UV.

DOI: 10.61011/TP.2025.10.62076.75-25

Introduction

Diffraction grating handbook [1] states that in 1893 M.A. Cornu understood that changes in the groove spacing changed the curvature of diffracted wavefronts and a classical plane grating would focus diffracted light if the grating was placed with a groove spacing „bias" M.A. Cornu checked this by placing three gratings, groove positions in which were set as varying when marking each groove. Such gratings where the straight parallel groove pattern has a variable, but clearly defined (though not periodic) spacing between successive grooves are now called varied line spacing (VLS) gratings.

To meet high resolution and performance requirements, diffraction gratings shall have a large uniform aperture, accurate groove positioning and improved groove shape. VLS gratings are often used in radiance conservation optics because they combine both diffraction and focusing capabilities in a single optical component [2]. VLS grating groove density varies over the grating length according to the polynomial law given as

$$p_x = mp_0 + mp_1 \cdot x + mp_2 \cdot x^2 + mp_3 \cdot x^3 + mp_4 \cdot x^4, \quad (1)$$

where x is the spacing over the grating length, m is the grating diffraction order, p_i are the coefficients in the polynomial law equation. Accurate groove positioning is critical for a VLS grating because linear groove density variation over the grating length defines focusing and the quadratic term provides aberration control [2].

VLS gratings were first fabricated using an CNC linear mover of the ruling engine by F.M. Gerasimov and colleagues from the USSR [3] and T. Harada and colleagues from Japan [4,5]. Ruled VLS gratings were manufactured for a wide range of applications: concave normal incidence gratings with aberration correction for Seya-Namioka monochromators and optical demultiplexers; concave glazing incidence gratings with aberration correction for cosmic ray spectrometers; focusing glazing incidence grating for synchrotron monochromators and wavefront generators for visible interferometry of optical surfaces (particularly aspherical ones) [6].

Voronov et al. [2] reported about manufacturing of X-ray lamellar VLS grating prototypes with a groove density of 300 mm and 600 mm^{-1} using direct-write laser lithography (DWL) on the Heidelberg^{TM} DWL66 and DWL2000 lithography systems. Grating quality was evaluated by wavefront measurement using the Zygo^{TM} Fizeau interferometer. The accuracy of DWL gratings approaches that of holographic gratings and can meet the quality requirements for many optical spectroscopy applications. Voronov et al. [7] reported on fabrication of a lamellar VLS diffraction grating with a groove density of 200 mm^{-1} using the DWL66 lithography system. Groove positioning accuracy was confirmed by reference grating wavefront measurements and comparison with theoretical variation of the VLS grating groove density.

This 30×20 mm VLS grating is used in a synchrotron (SR) beam providing radiation for EUV lithography. Another paper of the same authors reports on the development of a high-accuracy diffraction gratings manufacturing process for high resolution X-ray spectroscopy [8]. The above-mentioned process is based on a set of nanotechnological approaches, including recording of a grating pattern with constant or variable groove spacing on a quartz plate using electron-beam lithography, pattern transfer onto a bulk workpiece by large-area nanoimprint followed by dry and/or wet etching to form the groove profile. High reliability of the nanoimprint transfer stage was validated by differential wavefront measurements. Using the proposed approach, the lamellar VLS grating with a groove density of $900\,\mathrm{mm}^{-1}$ was fabricated for the soft X-ray fluorescent spectrometer.

Blazed gratings have at least twice as high efficiency as lamellar one, and are unrivaled in high order diffraction. For example, Goray et al. [9] proposed using a nanoimprint replica of the high frequency ($5000\,\mathrm{mm}^{-1}$) VLS blazed grating as the spectral purity filter for EUV lithography. The Mo-coated replica with a mean blaze angle of $\sim 13^\circ$ was made from the master with a blaze angle of 7.5° fabricated by wet etching of a Si wafer [10]. Theoretical efficiency of a conical diffraction grating taking into account the AFM-measured groove profile and RMS roughness of 0.5 nm was more than 80 % in minus-first-order (TM polarization) at 13.5 nm. Experimental efficiency of the same grating measured at a wavelength of 2.5 nm in conical diffraction was ~ 45 % [11]. Voronov et al. [12] developed a manufacturing process for creating VLS blazed gratings with a high groove density for high resolution X-ray spectroscopy using a set of nanodesign techniques, including electron-beam lithography, nanoimprint, anisotropic wet etching and plasma etching. The authors [12] report on manufacturing of two full-size high-frequency X-ray VLS gratings with blaze angles of 2.55 and 2.70°, groove density of 3000 mm and $6000\,\mathrm{mm}^{-1}$, optimized for the 1st and 2nd negative diffraction orders, respectively, for a resonance inelastic X-ray scattering (RIXS) spectrometer project at the Qerlin work station of the Advanced Light Source synchrotron. The groove positioning accuracy was confirmed by wavefront measurements on a reference grating recorded simultaneously with the VLS grating. The authors [12] also have found that inclusion of the 3rd and 4th order polynomial terms (see equation (1)) was not required for these gratings to achieve a high quality image.

High-resolution extreme UV and soft X-ray (SXR) monochromators and spectrometers used at 4th generation SR endstations and free-electron lasers, as well for planned numerous space missions require next generation high-efficiency and high-power-radiation resistant diffraction gratings. At this point it is generally recognized that „blazed“ gratings (with asymmetric triangular groove profile) made on vicinal Si wafers using anisotropic wet etching are the case [13–16].

Depending on the used lithography technique (electronic, laser, photolithography, etc.), this technology can be used to manufacture gratings with periods from several tens of nanometers to a hundred of micrometers and blaze angles from 0.04° to 70°. Obtained Si diffraction gratings feature a perfect triangular groove profile shape and the subatomic roughness level, and may be widely used in devices: 1) designed for any spectrum orders, including very high ones (echelle X-ray gratings [17]); 2) with the ultrahigh resolution $\sim 10^{-6}$ (for RIXS) [18]; 3) with the highest signal-to noise ratio $\sim 10^7 - 10^8$. In particular, for such grating with a period of $2\,\mu$m and a multilayer coating of Mo/Si, the record-breaking absolute efficiency of 40 % at 13.5 nm in the -8th order of nonpolarized radiation was achieved [19].

Due to the unsolved problem of removing nubs on triangular groove profile ridges of blazed gratings, investigations for the achievement of high X-ray resolution have been recently focused mainly on the development of gratings with high and ultrahigh groove densities. As to our group, the problem of removing Si nubs was solved and the main focus was made on fabrication of gratings with low and medium groove densities. It has been found [17] that attainability of a high order diffraction of a blazed grating depended on the reflecting facet flatness, for characterization of which a camber parameter was proposed. The difference of inclination angles of the top (α_2) and bottom (α_1) parts of the reflecting facet $C = \alpha_2 - \alpha_1$ measured taking into account 30 % of top profile points and 30 % of bottom profile points, dropping 10 % profile points from the lowest point, is assumed as the reflecting facet camber (C). Low camber of the reflecting facet of a blazed grating groove is provided by a previously developed technique [20].

This work describes the details of manufacturing process and properties of two VLS gratings with a groove density of $\sim 500\,\mathrm{mm}^{-1}$ and two different reflecting facet inclination angles (blaze angles).

1. VLS grating design

The developed VLS grating is designed for a polychromator used in the solar-bling UV range with a central wavelength of 275 nm. To achieve the high resolution, a grating with an ultrahigh groove density or a medium-frequency high diffraction order grating is necessary. A high diffraction order for achievement of high/ultrahigh resolution of a medium-frequency grating is defined as the order that satisfies $|n| \gtrsim 10$. Such grating diffraction orders may be achieved by meeting some conditions: first, the total absence of Si nubs on the triangular profile ridge; second, a flat (not curved) reflecting facet. Both conditions may be achieved by means of smoothing etching performed after anisotropic etching of grooves in KOH using the previously developed technique [20].

According to preliminary calculations in PCGrate^{TM} [21], the maximum absolute spectral efficiency of a medium-frequency grating with a period of $2\,\mu$m and a blaze angle of 42.5° for nonpolarized radiation is 33.5 % in the -10th order

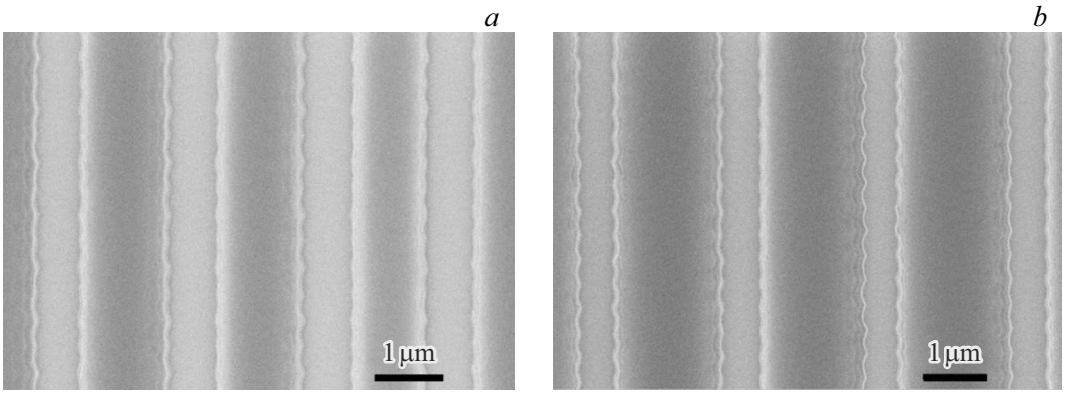

Figure 1. SEM images with a magnification of 40 K, a plan view of the PR mask of VLS grating № 2 linear: *a* — at the beginning of the aperture; *b* — at the end of the aperture. Dark bands are strips of the PR mask, bright bands are gaps in the PR mask (unprotected Si).

($n = -10$). The design of the UV polychromator requires a VLS grating with a groove density of $p_x = mp_0 + mp_1 \cdot x + mp_2 \cdot x^2 + mp_3 \cdot x^3 + mp_4 \cdot x^4$, where polynomial coefficients are equal to: $P_0 = 466.08\,\text{mm}^{-1}$; $P_1 = 3.163\,\text{mm}^{-2}$; $P_2 = -0.0491\,\text{mm}^{-3}$; $P_3 = -0.785 \cdot 10^{-3}\,\text{mm}^{-4}$; $P_4 = -1.636 \cdot 10^{-5}\,\text{mm}^{-5}$. The total grating length is 30 mm, distance to the left/right of the center of grating is 15 mm each, period varies over the grating aperture by $\sim 20\,\%$.

To streamline manufacturing processes, it was decided to make two gratings as VLS grating prototypes with a groove density $\sim 500\,\text{mm}^{-1}$: grating № 1 with asymmetric triangular profile and a small blaze angle of $\sim 4^\circ$ and grating № 2 with the almost symmetric triangular profile and large reflecting facet inclination angle 50.7°. Vicinal Si wafers with a diameter of 3″ were used for manufacturing: Si(111)4° for VLS grating № 1 and Si(100)4° for grating № 2. Grooved region size is 30×12 mm.

2. Fabrication and characterization of VLS gratings

2.1. Protective mask pattern formation

The first task was to form a VLS grating mask pattern using the direct-write lithography. According to the calculation, the groove density over the VLS grating length varies from $500\,\text{mm}^{-1}$ to $410\,\text{mm}^{-1}$. Taking into account the smallness of p_2, it was decided to manufacture for comparing one of the VLS grating prototypes with linear period variation.

For grating № 1, a mask pattern with only linear variation of the groove density was recorded, and for grating № 2, two mask patterns were recorded: with linear variation and polynomial variation of the groove density considering coefficients up to p_4, inclusive.

The quality of a photoresist mask (PR mask) formed using direct-write lithography defines the quality of a future VLS grating. A groove positioning accuracy is the key property of diffraction gratings. It is critical to adhere accuracy requirements to the groove density distribution for VLS gratings because they provide focusing and corrections of low order aberrations of the spectrometer optics. Since $20\,\mu$m wide strips are used to record a pattern on a laser lithography system, there might be a problem with potential errors of groove crosslinking at strip boundaries.

A Si wafer was spin-coated with resist and then preliminary baked. A grating pattern was recorded using the direct-write lithography system with a focused laser beam ($\lambda = 405$ nm) by scanning on the Si wafer coated with resist. The required pattern was achieved by moving a table with the wafer with a predefined laser beam intensity during recording. Under preliminary experiments, the laser beam intensity was chosen for recording a PR mask pattern to provide the desired width of exposed resist strips that are later dissolved as the PR mask is developed and uncover the Si surface. At the following stage, a chromium layer was deposited on the wafer with the created resist mask.

Figure 1 shows SEM plan view images of the PR mask at the beginning (Figure 1, *a*) and at the end (Figure 1, *b*) over the length of linear VLS grating № 2 (hereinafter referred to as 'linear').

A Cr mask on the Si wafer surface was formed by lift-off of the metal layer with the PR mask: the samples with developed PR mask were coated with a vacuum-sputtered 20 nm chromium layer that was later lifted off by treatment in dimethylformamide. To remove the resist residues, the samples were treated by oxygen plasma.

Photograph of the Cr mask of grating № 2 is shown in Figure 2, polynomial grating № 2 (hereinafter referred to as 'polynomial') is placed closer to the primary flat, the linear grating is placed farther from the wafer primary flat.

For gratings with a period varying over the grating length, it is important to choose the best width of Cr strips of the protective mask: too narrow Cr strips do not ensure protection during anisotropic etching in a KOH solution; too wide Cr strips increase the etching time to achieve the desired blaze angle. A spacing between Cr mask strips (the etching space) defines the etching depth, therefore, the

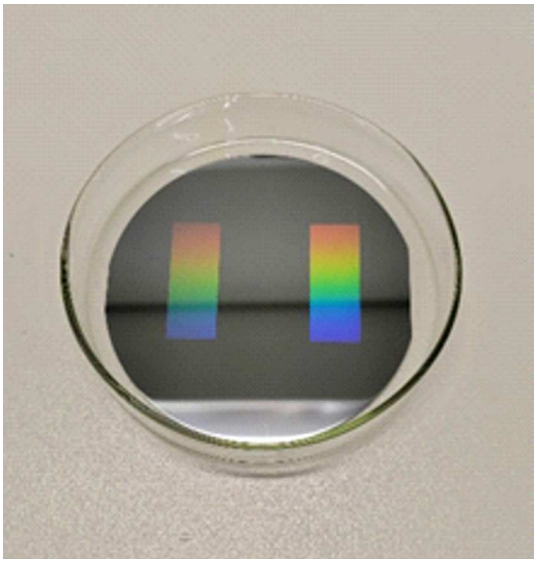

Figure 2. Photograph of the Cr mask of grating № 2: near the primary flat ('polynomial'), farther from the primary flat ('linear'.

etching depth will be different for different etching spaces with the same etching time.

Grating № 1. The Cr strip width of the etching mask varies from 754 nm (the narrowest strip) to 994 nm (the widest strip), the mean width of Cr strips throughout the grating length is 888 nm.

Grating № 2. 'Linear': the Cr strip width varies from 835 nm (the narrowest strip) to 1165 nm (the widest strip), mean width of Cr strips throughout the grating length is 1013 nm.

'Polynomial': the Cr strip width varies from 820 nm (the narrowest strip) to 1121 nm (the widest strip), mean width of Cr strips of the protective mask throughout the grating length is 1009 nm. Figure 3 shows SEM plan view images of the Cr mask at the beginning (Figure 3, *a*) and at the end (Figure 3, *b*) over the length of linear VLS grating № 2.

2.2. Groove etching

For anisotropic etching in a 20 mass% KOH solution, such an etching time shall be chosen so that to achieve the same designed blaze angle throughout the VLS grating region. Therefore the actual grating etching time was virtually twice longer than the time that is theoretically necessary to achieve the calculated etching depth.

Grating № 1. The gaps for etching vary from 1120 nm to 1559 nm (the range is 439 nm). The groove etching depth varies over the length of grating № 1 from 232 to 265 nm (Figure 4, upper profiles).

During anisotropic etching of grooves with a small inclination angle, Si nubs are formed on the triangular profile ridge as a result of side etching of Si under the protective Cr mask. We have earlier developed and improved the technique to be used for Si nubs removal and polishing of reflecting facet surfaces of blazed gratings by etching in the smoothing and polishing etchant [17]. This technique may be used to make blazed gratings with flat (not curved) reflecting facet of a groove to achieve high diffraction orders, with the -10th order required in our case.

Si nubs in heights of 150−154 nm and in widths of 220−274 nm on the profile of grating № 1 were removed by etching in the smoothing and polishing etchant (Figure 4, lower profiles). Adequacy of smoothing and polishing etching was inspected using SEM plan view images over the Si nubs width. Then the grating was cleaned by treatment in a piranha solution ($H_2SO_4 + H_2O_2$).

Grating № 2. The gaps for etching vary from 987 nm to 1430 nm (the range is 443 nm). SEM plan view images of grating № 2 linear recorded after etching in KOH with the Cr mask during the calculated time (Figure 5, *a*) show that the grating was not etched to the preset depth. Figure 5, *a* shows irregularly shaped particles on the grating surface — these are Si etching products that were later removed. The adhesion of the Cr mask to Si on the grating surface was good: after anisotropic etching in a 20 % KOH solution the Cr mask was not separated during the calculated time. Additional etching was required to achieve the desired etching depth (Figure 5, *b*). The groove blaze angle after additional etching of grating № 2 linear varied from $\sim 42^\circ$ to $\sim 49^\circ$.

During anisotropic alkaline etching of grooves of an almost symmetric grating with the large blaze angle, Si nubs are not formed on the triangular profile ridge, but flats are formed by Cr mask strips. It is important to choose such a Cr mask strip width so that Si under Cr is completely etched away to the desired angle as a result of side etching during the groove etching time, and narrow pads 141−187 nm in width and/or sharp (slightly rounded) edges (Figure 6, *b, d*) were formed on the profile ridge instead of flats 727−750 nm in width (Figure 6, *a, c*).

2.3. Grating characteristics

SEM photographs were made with different magnifications (40 000× and 50 000×) using the Zeiss^{TM} Supra 25 scanning electron microscope; panoramic SEM images were recorded with 5000× magnification. Grating profiles were examined using the Veeco^{TM} Dimension 3100 atomic-force microscope in the semi-contact (or tapping) mode; all scans contained 512 × 512 points. TipsNano^{TM} silicon probes with a typical rounding radius of < 10 nm were used.

Grating № 1. After removal of Si nubs, the period and the antireflective facet width of grating № 1 were measured using the SEM method (Figure 7). The antireflective facet width varies in the range from 276 nm to 231 nm over the grating length that amounts to 13.9−9.6 % of the period.

Table 1 shows the AFM measurements of grating № 1 parameters at various fabrication stages; for comparison the grating period was also measured using SEM.

Gratinng№ 2. Table 2 shows the AFM measurements of grating № 2 parameters with the linear groove density

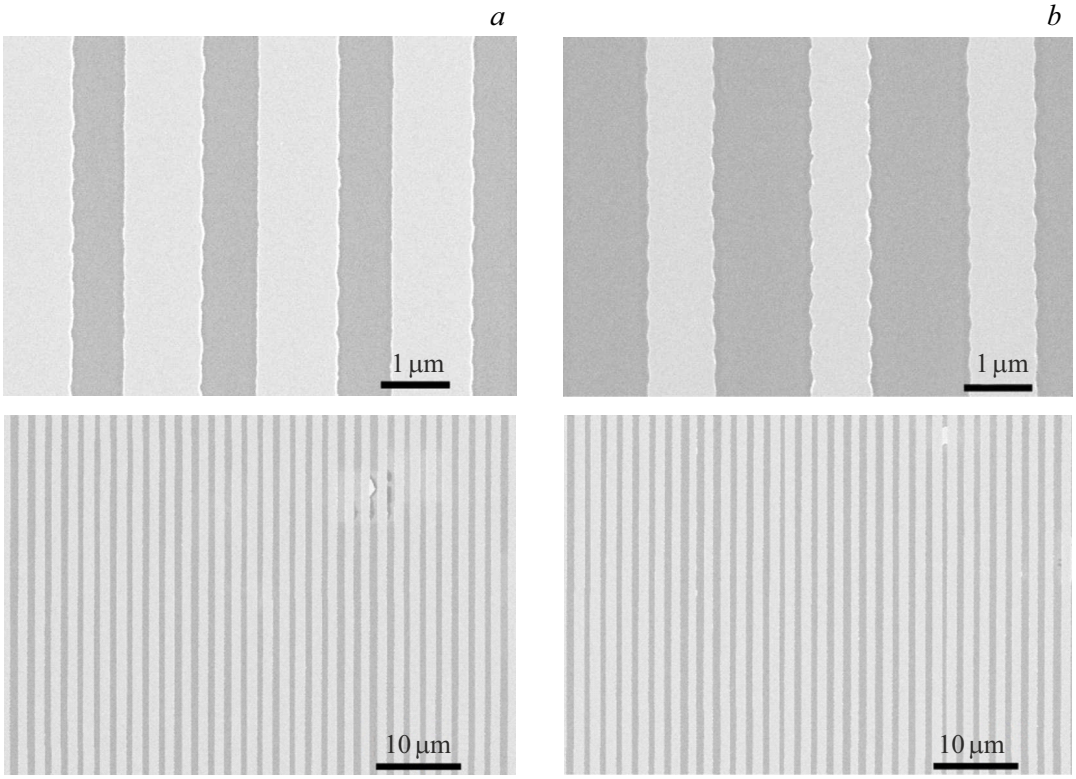

Figure 3. SEM images with 40 K and 5 K magnifications, plan view of the Cr mask of VLS grating № 2 linear: *a* — at the beginning of the aperture; *b* — at the end of the aperture. Bright bands are the Cr mask strips, dark bands are the gaps for etching (unprotected Si).

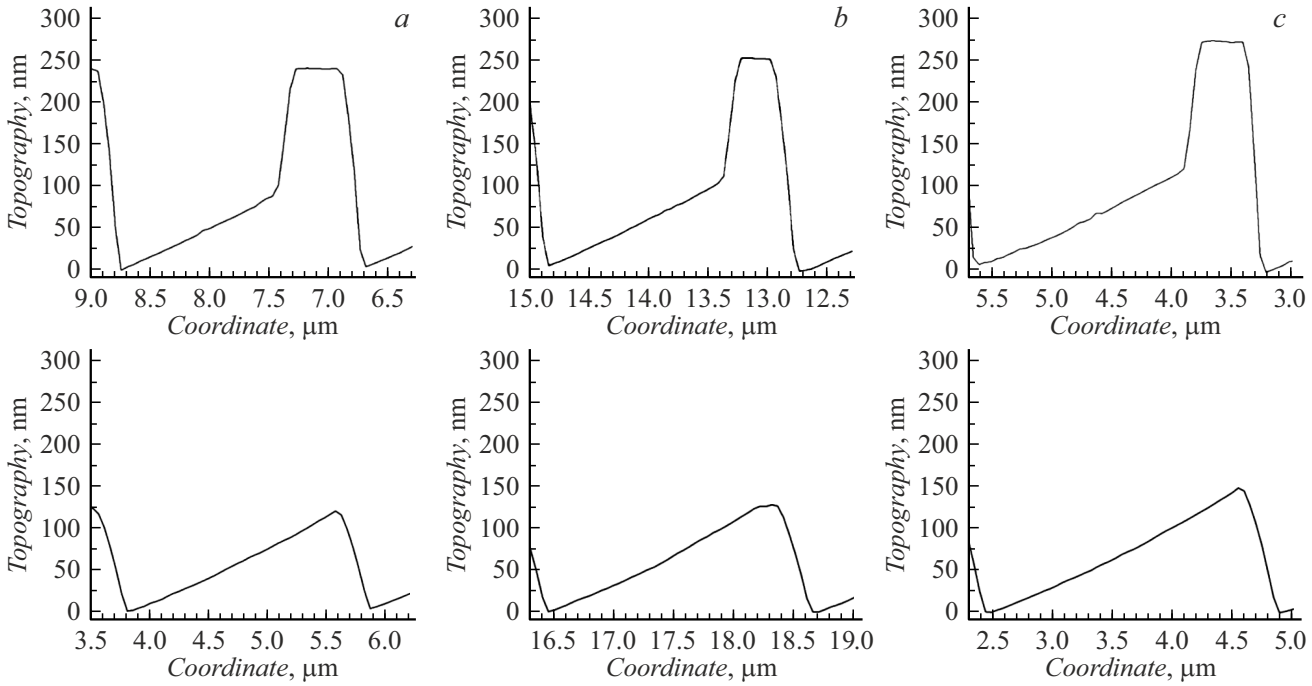

Figure 4. AFM profiles of grating № 1 after etching in KOH (upper profiles) and after removal of nubs (lower profiles) in the region: *a* — at the beginning, *b* — at the middle, *c* — at the end.

variation; for comparison the grating period was also measured using SEM.

Table 3 shows the AFM measurements of grating № 2 parameters with the polynomial groove density variation;

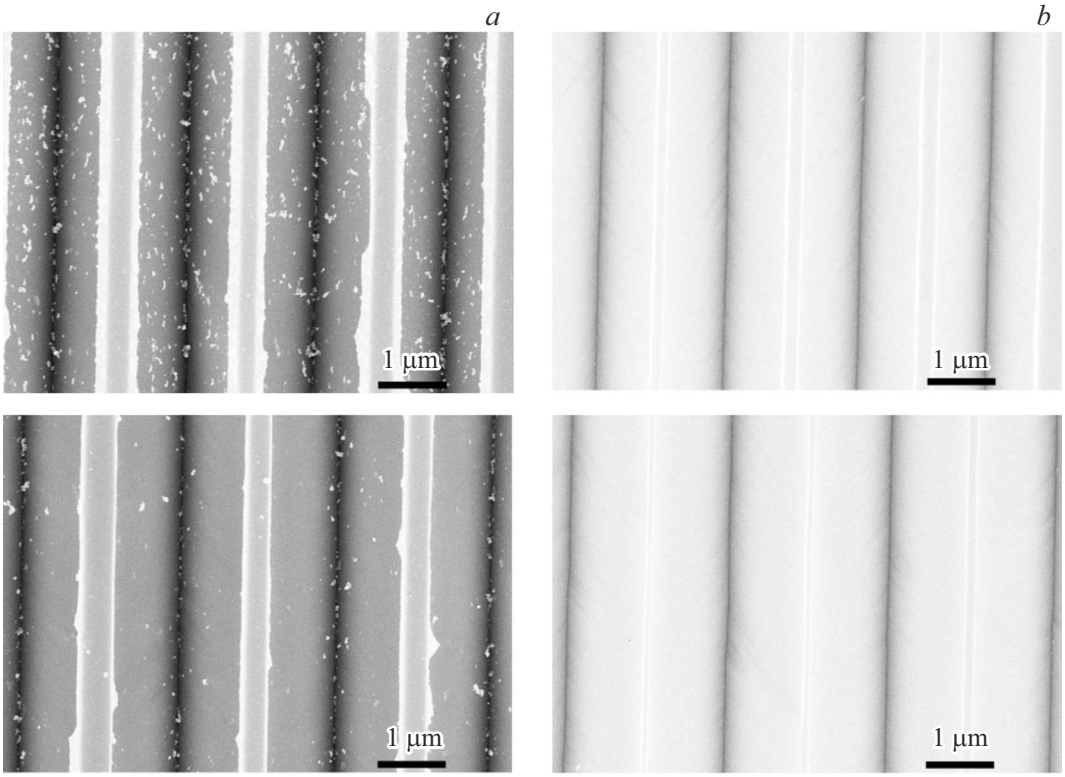

Figure 5. SEM plan view images at the beginning of the aperture (upper images) and at the end of the aperture (lower images) of VLS grating № 2 linear after etching in KOH with the Cr mask: *a* — within the calculated time; *b* — after additional etching and Cr mask removal.

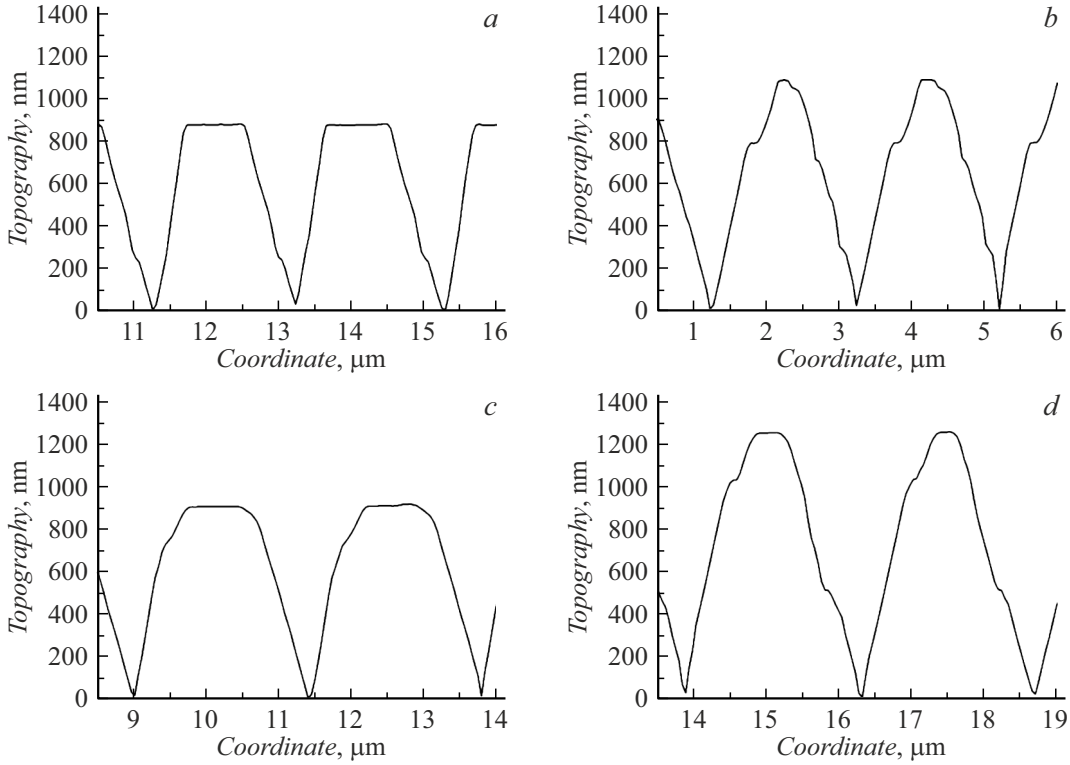

Figure 6. AFM profiles of VLS grating № 2 linear after etching in KOH with the Cr mask: *a* and *c* — within the calculated time; *b* and *d* — after additional etching.

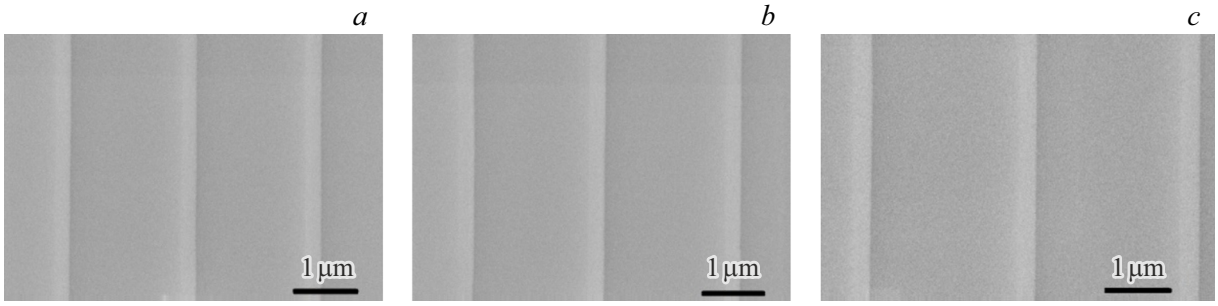

Figure 7. SEM images at 50 K, plan view of grating № 1 after removal of Si nubs: *a* — at the beginning, *b* — at the middle, *c* — at the end.

Table 1. Measurements of grating № 1

Grating region and measurement method	Period, μm				Blaze angle, °	Camber, °	Antiblaze, angle, °	Groove depth, nm
	After etching in KOH		After nubs removal					
	SEM	AFM	SEM	AFM				
beginning	1.97	2.00	1.98	2.00	3.78	0.79	26.3	119
Middle	2.11	2.15	2.07	2.14	3.86	1.09	25.9	124
End	2.39	2.45	2.41	2.45	3.91	0.96	27.4	144

for comparison the grating period was also measured using SEM.

3. Results and discussion

When the groove density varies linearly from 500 mm to 410 mm^{-1}, the theoretically calculated grating period shall vary from 1.95 μm to 2.39 μm, and when the groove density varies polynomially, the grating period shall vary from 2.04 μm to 2.44 μm.

Grating № 1. As shown in Table 1, the period of grating № 1 varies from 1.99 μm to 2.43 μm that is satisfactory. The mean blaze angle of grating № 1 is 3.85°. Grating № 1 has a triangular asymmetric profile free of nubs, but non-ideal. First, Figure 4, *a, b* (lower profiles) shows that the profile ridge has rounding tending to form a flat. Second, the reflecting facet is not flat, but is curved up to 1.1°, though the high diffraction order for this grating may be achieved only with the absolute camber not greater than $\sim 0.4°$. In [14], it was shown that the maximum efficiency of high diffraction orders ($|n| \gtrsim 10$) of the fabricated echelle gratings might be achieved in real practice only when the reflecting facet camber c was $\leq 10\,\%$ of the mean blaze angle, i.e. the relative camber $C \leq 0.1\alpha$. The groove profile imperfections are associated with the fact that Si nubs parameters at the beginning and end of the grating aperture after grating etching in KOH differed greatly: the groove etching depth difference was ~ 33 nm, the Si nub width difference was ~ 54 nm, and the Si nub height was more than 50 % of the total groove etching depth because the etching time was much longer than required for groove etching in a constant-period grating. Therefore the sufficiently long smoothing etching time was chosen to enable removal of wider Si nubs simultaneously with narrow ones. However, since the width of narrow and wide Si nubs differs by 12 %, the time turned out to be non-optimum, too long, for grating regions with narrower Si nubs, and, consequently, the reflecting facet length in these regions of grating № 1 slightly decreased. As can be seen from the results provided in Section 3, the VLS grating smoothing procedure is to be improved to achieve satisfactory flatness of the reflecting facet of a groove.

Fabricated grating № 1 is a very interesting object for future investigation of its diffraction efficiency because the blaze angle is virtually the same over the aperture, and the reflecting facet length and curvature are different throughout the VLS grating aperture. It would be interesting to explore how much the diffraction efficiency decreases in the chosen order depending on the reflecting facet length of the VLS grating, and to determine a maximum allowable high-efficiency diffraction order number at the beginning, in the middle and at the end of the VLS grating aperture. For this, diffraction efficiency of the VLS grating shall be determined by simulation in a PCGrate^{TM} code using the boundary integral equation method and groove profiles measured by AFM in various grating regions (beginning, middle, end). This will be done during ongoing investigations of the fabricated VLS gratings.

Grating № 2. As shown in Table 2, the period of grating № 2 linear varies from 1.95 μm to 2.38 μm that coincides with the preset values. The mean blaze angle of grating № 2 linear is 48.9°, which is slightly smaller than the preset blaze angle (by 1.8°). The groove profile of grating № 2 linear is almost symmetric, triangular, but non-ideal: as can be seen in Figure 6, *b, d*, instead of a flat, the profile ridge has a small rounded pad, whose width is five time smaller.

Table 2. Measurements of grating № 2 linear

Grating region and measurement method	period, μm		Blaze angle, °
	SEM	AFM	
Beginning	1.92	1.95	47.8
End	2.32	2.38	50.6

Table 3. Measurements of grating № 2 linear

Grating region and measurement method	period, μm		Blaze angle, °
	SEM	AFM	
Beginning	1.97	1.97	45.5
End	2.39	2.42	46.5

As shown in Table 3, the period of grating № 2 polynomial varies from 1.97 μm to 2.42 μm, while the initial value is slightly smaller than the calculated value. The mean blaze angle of grating № 2 polynomial is 46.0°, which differs very much from the preset blaze angle (by 4.7°). The groove profile of grating № 2 polynomial is almost symmetric, triangular, but non-ideal: the profile ridge still has flats, whose width is only two and a half times smaller.

As it follows from the results given in Section 3, the etching process of VLS gratings with the large blaze angle shall be improved.

Conclusion

Fabrication of solar-blind UV diffraction gratings was streamlined using the direct-write lithography technique. The problem of fabrication of gratings with a variable groove density according to a predetermined law was generally successfully solved. Several 30×12 mm VLS grating prototypes having the asymmetric triangular profile with small blaze angle and the almost symmetric triangular profile with large blaze angle, groove density of which varied both linearly and polynomially, were fabricated. It is planned to perform interferometric wavefront measurements of the fabricated diffraction grating prototypes and to clarify their diffraction efficiency. Using the results provided in the work and ongoing investigations, it is possible to make a silicon VLS grating with the desired groove density variation, high efficiency and low scattered light level for the UV polychromator.

Funding

The study was partially supported by the Ministry of Science and Higher Education of the Russian Federation (FSRM-2023-0006). The study performed by D.V. Mokhov, L.I. Goray and A.D. Buravleuv was supported by the Russian Science Foundation in the theoretical part (№ 25-12-00139).

Conflict of interest

The authors declare no conflict of interest.

References

[1] C. Palmer. *Diffraction grating handbook eighth edition* (MKS Instruments, Inc., NY., USA, 2020)
[2] D.L. Voronov, S. Diez, P. Lum, S.A. Hidalgo, T. Warwick, N. Artemiev, H.A. Padmore. Proc. SPIE, **8848**, 88480 (2013). DOI: 10.1117/12.2024489
[3] F.M. Gerasimov, E.A. Yakovlev, I.V. Peisakhson, B.V. Koshelev. Opt. i spektr., **28** (4), 790 (1970) (in Russian).
[4] T. Harada, T. Kita. Appl. Opt., **19** (23), 3987 (1980). https://doi.org/10.1364/AO.19.003987
[5] M. Itou, T. Harada, T. Kita. Appl. Opt., **28** (1), 146 (1989). https://doi.org/10.1364/AO.28.000146
[6] M.C. Hettrick. Proc. SPIE 0560, Diffraction Phenomena in Optical Engineering Applications, (1986). https://doi.org/10.1117/12.949620
[7] D.L. Voronov, T. Warwick, E.M. Gullikson, F. Salmassi, P. Naulleau, N.A. Artemiev, P. Lum, H.A. Padmore. Proc. SPIE, **9207**, 920706 (2014). DOI: 10.1117/12.2062340
[8] D.L. Voronov, E.M. Gullikson, H.A. Padmore. Opt. Express, **25** (19), 23334 (2017). https://doi.org/10.1364/OE.25.023334
[9] L.I. Goray. Proc. SPIE, **6317**, 631700 (2006). DOI: 10.1117/12.678151
[10] J.F. Seely, L.I. Goray, B. Kjornrattanawanich, J.M. Laming, G.E. Holland, K.A. Flanagan, R.K. Heilmann, C.H. Chang, M.L. Schattenburg, A.P. Rasmussen. Appl. Opt., **45** (8), 1680 (2006). DOI: 10.1364/AO.45.001680
[11] C.-H. Chang, J.C. Montoya, M. Akilian, A. Lapsa, R.K. Heilmann, M.L. Schattenburg. J. Vac. Sci. Technol. B, **22** (6), 3260 (2004). DOI: 10.1116/1.1809614
[12] D.L. Voronov, S. Park, E.M. Gullikson, F. Salmassi, H.A. Padmore. Opt. Express, **30** (16), (2022). https://doi.org/10.1364/OE.460740
[13] R.K. Heilmann, D.P. Huenemoerder, J.A. McCoy, R.L. McEntaffer. arXiv:2409.02297v1. (2024).
[14] L. Golub, P. Cheimets, E.E. DeLuca, Chad A. Madsen, K.K. Reeves, J. Samra, S. Savage, A. Winebarger, A.R. Bruccoleri. J. Space Weather Space Clim., **10**, 37 (2020).
[15] D.L. Voronov, L.I. Goray, T. Warwick, V. Yaschuk, H.A. Padmore. Opt. Express, **23** (4), 4771 (2015).
[16] X. Haoyu, J. Yanxiu, C. Xingshuo, W. Ruipeng, Z. Jing, Chin. J. Opt., **17** (5), 1139 (2024).
[17] L.I. Goray, T.N. Berezovskaya, D.V. Mokhov, V.A. Sharov, K.Yu. Shubina, E.V. Pirogov, A.S. Dashkov. J. Surf. Inv.: X-ray, Syn. & Neut. Tech., **17** (1), S104 (2023). DOI: 10.1134/S1027451023070145
[18] D.L. Voronov, E.H. Anderson, R. Cambie, S. Cabrini, S.D. Dhuey, L.I. Goray, E.M. Gullikson, F. Salmassi, T. Warwick, V.V. Yashchuk, H.A. Padmore. Opt. Express, **19**, 6320 (2011). https://doi.org/10.1364/OE.19.006320

[19] L.I. Goray, T.N. Berezovskaya, D.V. Mokhov, V.A. Sharov, K.Yu. Shubina, E.V. Pirogov, A.S. Dashkov, A.V. Nashchekin, M.V. Zorina, M.M. Barysheva, S.A. Garakhin, S.Yu. Zuev, N.I. Chkhalo. Bull. Lebed. Phys. Inst., **50** (2), S250 (2023).
[20] D.V. Mokhov, T.N. Berezovskaya, K.Yu. Shubina, E.V. Pirogov, A.V. Nashchekin, V.A. Sharov, L.I. Goray. Tech. Phys., **68** (1), S96 (2023). DOI: 10.1134/S1063784223090116
[21] L.I. Goray, S.Yu. Sadov. Computer code PCGrate™ [Web resource]. URL: http://pcgrate.com (date of access 20.10.2024)

Translated by E.Ilinskaya